



Photothermal effects and toxicity of Fe₃O₄ nanoparticles *via* near infrared laser irradiation for cancer therapy



Andrew W. Dunn^a, Sadat M. Ehsan^b, David Mast^b, Giovanni M. Pauletti^c, Hong Xu^d, Jiaming Zhang^e, Rodney C. Ewing^e, Donglu Shi^{a,f,*}

^a The Materials Science and Engineering Program, Dept. of Mechanical and Materials Engineering, College of Engineering and Applied Science, University of Cincinnati, Cincinnati, OH 45221, USA

^b Department of Physics, University of Cincinnati, Cincinnati, OH 45221, USA

^c The James L. Winkle College of Pharmacy, University of Cincinnati, Cincinnati, OH 45267, USA

^d Nano Biomedical Research Center, School of Biomedical Engineering, Med-X Research Institute, Shanghai Jiao Tong University, Shanghai 200030, China

^e Department of Geological & Environmental Sciences, Stanford University, Stanford, CA 94305, USA

^f Shanghai East Hospital, The Institute for Biomedical Engineering & Nano Science, Tongji University School of Medicine, Shanghai 200120, China

ARTICLE INFO

Article history:

Received 3 June 2014

Received in revised form 9 September 2014

Accepted 30 September 2014

Available online 7 October 2014

Keywords:

Nanotechnology
Nanomedicine
Cancer therapy
Photothermal effect
Hyperthermia

ABSTRACT

The photothermal effect of magnetite (Fe₃O₄) nanoparticles was characterized by photonic absorption in the near-infrared (NIR) region. Upon laser irradiation at 785 nm, the Fe₃O₄ nanoparticles generate localized hyperthermia in tumorous lesions, which is an effective strategy for cancer therapy; however, uncoated magnetite possesses an innate toxicity which can lead to drawbacks in the clinical setting. To reduce innate toxicity, a poly(acrylic acid) (PAA) coating on the nanoparticles was investigated in order to determine the alterations to stability and the degree of toxicity in an attempt to create a higher utility vector. It was found that the PAA coating significantly reduced the innate toxicity of the uncoated magnetite. Furthermore, the efficacy of PAA-coated magnetite nanoparticles (PAA-Fe₃O₄) was investigated for treating MDA-MB-231 (human mammary gland adenocarcinoma) cultures in viable concentration ranges (0.1–0.5 mg/ml). An appropriate PAA-Fe₃O₄ concentration range was then established for inducing significant cell death by hyperthermic ablation, but not through innate toxicity.

© 2014 Elsevier B.V. All rights reserved.

1. Introduction

The development of minimally invasive cancer treatments by the effective delivery of drug “payloads” to targeted lesions is of great interest to oncologists. The photothermal effect of Fe₃O₄ nanoparticles has been recently discovered and investigated for applicability in tumor treatments [1–8]. Upon near-infrared laser irradiation, the Fe₃O₄ magnetic nanoparticles generate sufficient energy to thermally ablate cancer cells. The main advantages of photothermal treatment are easy modifications to application areas and manipulation of thermal energy in targeted regions. This ease of application and manipulation of thermal energy generation requires that localized uptake of the nanoparticles reaches a sufficient concentration applicable for optical hyperthermia. A concern in clinical studies is that the innate toxicity of nanoparticle complexes at concentrations required for sufficient thermal energy generation proves to be significant. Investigations on the concentration dependent innate toxicity of uncoated magnetite nanoparticles have shown a significant impact on cellular viability for several types of cell lines. For the murine macrophage cell line J774 and glial cell line

SVGp12, pronounced toxicity is observed beginning at 100 µg/ml [9, 10]. However as iron oxide nanoparticle species have been previously shown to produce reactive oxygen species (ROS) through the release of free iron ions *in-vitro*, light-activated release of ROS species by photosensitizers coupled to the nanoparticle surface or protective surface coatings may improve photodynamic efficacy by reducing the required concentration required for elicitation of significant toxicity upon electromagnetic irradiation or by reducing innate toxicity [11–15].

The elevated vasculature endothelial growth and permeability factors mixed with disrupted endothelial, media, and adventitia layers, lead to leaky vasculature that is not usually seen in normal, healthy tissue [16–18]. As such, preferential accumulation of nanoparticle systems will occur in tumor tissue that provides a 10–50 fold increase in local concentration within 1–2 days [16]. Conveniently the nanoparticles in the endocytotic size range (<100 nm) exist within the size range for utilization of enhanced permeability and retention (EPR) effect [16,18–20]. This suggests that nanoparticles designed to utilize the EPR effect are likely to become internalized by cell lines once the nanoparticles leave the vasculature and, based on their size, become sequestered in lysosomal and other endosomal compartments. However, the EPR effect is not solely restricted to solid tumor masses and is observed in other inflammatory regions [17]. It is therefore critical

* Corresponding author.
E-mail address: donglu.shi@uc.edu (D. Shi).

that the concentration of nanoparticles be optimized in regions that experience the EPR effect, either cancerous or non-cancerous, such that the innate toxicity is minimized. Moreover upon the controlled application of mediating factors, significant toxicity during treatment may be elicited thereby allowing a highly efficacious and selective treatment regimen [1,7,21].

Quantification of innate toxicity reduction of uncoated magnetite nanoparticles (UC-Fe₃O₄) utilizing a one-pot, hydrothermal synthesis method for the surface deposition of poly(acrylic acid) (PAA) was investigated on MDA-MB-231 (human mammary gland adenocarcinoma) cultures. Furthermore, the size, colloidal stability, and photothermal effect under near-infrared irradiation of poly(acrylic acid)-coated magnetite nanoparticles (PAA-Fe₃O₄) and the UC-Fe₃O₄ variant were investigated for determination of the applicability of the chosen synthesis method and capping agent of the magnetite species for future *in-vivo* optical hyperthermia.

2. Methods

2.1. Nanoparticle synthesis

The PAA-coated, Fe₃O₄ nanoparticles were prepared by the polyol method as reported in a previous study. A 3 mM FeCl₃·6H₂O solution was completely dissolved in ethylene glycol and homogenized through ultrasonication and vigorous stirring. A solution of 4 mM poly(acrylic acid), deionized water, and 0.3 M urea was then added. The mixture was further ultrasonicated for 10 min and then sealed in a Teflon-lined, stainless-steel 50 ml autoclave vessel. The autoclave vessel was then heated to 200 °C for 12 h and then allowed to cool to room temperature. Newly formed PAA-Fe₃O₄ nanoparticles were isolated through magnetic separation and washed several times with water and ethanol to removed inorganic and organic impurities [22].

For UC-Fe₃O₄, 0.01 M FeCl₂·6H₂O and 0.02 M FeCl₃·6H₂O were dissolved in distilled 6H₂O at 80 °C under nitrogen through stirring. After 60 min, NaOH was added to the mixture. The mixture was then stirred for a further 2 h at 90 °C under nitrogen.

2.2. Characterization

UC-Fe₃O₄ and PAA-Fe₃O₄ nanoparticles were dispersed in complete-DMEM, HBSS and DI-water. Size was quantified through dynamic light scattering conducted on a Zetasizer Nano ZS (Malvern Instruments, Ltd.) using the nanoparticles dispersed in complete-DMEM to mimic *in vivo* conditions and in HBSS for stability comparison. Solutions were maintained at 37 °C for the duration of characterization. Zeta potential was measured by electrophoretic light scattering conducted by a Zetasizer Nano ZS (Malvern Instruments, Ltd.) using the nanoparticles dispersed in purified deionized water (DI-water). X-ray diffraction of UC-Fe₃O₄ and PAA-Fe₃O₄ nanoparticles has been previously conducted [22].

2.3. Growth media

High glucose Dulbecco's Modified Eagle's Medium (DMEM) (HyClone, Fisher Scientific) was obtained from the Fisher Scientific. Each container stored 500 ml of DMEM mixed with 7.00 mM L-glutamine and 2250 mg of glucose, without sodium pyruvate. Growth media were completed with 50 ml of fetal bovine serum (FBS) (Atlanta Biologicals), 5 ml of penicillin/streptomycin (HyClone, Fisher Scientific), 5 ml of minimum essential medium (MEM), non-essential amino acids 100× concentration (CellGro, Mediatech Inc.), and 5 ml of L-glutamine (CellGro, Mediatech Inc.).

2.4. Hank's balanced salt solution

500 ml of de-ionized water was heated in an autoclave in a glass jar for 30 min. After sterilization the glass jar was allowed to rest for a minimum of 24 h to achieve room temperature. The following components were massed to be added to 100 ml of the sterilized de-ionized water: 0.98 g of HBSS mixture (Sigma-Aldrich), 0.037 g sodium bicarbonate (Fisher Scientific), 10.50 g D(+) glucose (Sigma-Aldrich), and 8.59 g HEPES (Sigma-Aldrich). Two 50 ml conical vials were used in the creation of 100 ml of HBSS. After the addition of all solutes, each 50 ml conical vial was then adjusted to a pH of 7.2 through the addition of a 1 M sodium hydroxide solution. Aliquots were taken from the two vials and further purified before use.

2.5. Nanoparticle solutions

UC-Fe₃O₄ and PAA-Fe₃O₄ stock solutions of 13.8 and 11.2 mg/ml were respectively used to create 7.5, 5, 2.5, and 1 mg/ml solutions prepared with complete-DMEM. Serial dilutions were performed starting with the 1 mg/ml solution to create 0.5, 0.2, 0.1, 0.05, 0.025, 0.01, 0.005, and 0.001 mg/ml prepared with complete-DMEM.

2.6. Cell culture

MDA-MB-231 human mammary gland adenocarcinoma tissue samples were acquired from the American Type Culture Collection. Samples were cultured in T75CN vent cap tissue culture flasks (Sarstedt) and were maintained at a constant temperature of 37 °C in a 5% CO₂ environment during culturing and testing. Splitting was performed with 3 ml of trypsin-EDTA 1× concentration (HyClone, Fisher Scientific).

2.7. Innate toxicity

96 white well plates were seeded with 100 µl of 30,000 cells/µl. After seeding, the 96 white well plates were incubated at 37 °C in a 5% CO₂ environment for 24 h to allow for cell adhesion. This cellular density was chosen so to disallow complete confluency of any of the seeded wells by the end of the innate toxicity experiment. MDA-MB-231 cultures in the 96 well plates were subjected to 100 µl of UC-Fe₃O₄ or PAA-Fe₃O₄ suspended in complete-DMEM after this 24 hour period and further incubated for 48 h at 37 °C. Following the 48 hour incubation period, the viability of each well was assessed using the CellTiter-Glo® luminescent cell viability assay (Promega). The lysis buffer was created per the Promega protocol. The 96 well plates were placed on an orbital shaker for 10 min following the addition of 100 µl of the completed lysis buffer to each test well. The plate was further allowed to rest for another 10 min before the quantification of luminescent output.

2.8. Photothermal ablation

A standard power meter (Coherent Inc.) was used to determine the relation between the applied current and the optical power output. A liner function was fit to the data to allow calculation of the laser power and consequent intensity over an applied area. For each PAA-coated magnetite nanoparticle concentration, laser intensity and wavelength used during MDA-MB-231 irradiation trials, a heating and cooling curve was generated. An infrared camera (FLIR-T640) was oriented to monitor the temperature of the nanoparticle solutions. For determination of the heating curve, temperatures were recorded every minute for the first 8 min and every 2 min for the next 12 min. The cooling curve was determined by recording the temperature at 30 s, 1 min, and every following minute for the next 7 min after removal of the laser. After establishing the appropriate laser intensity, hyperthermic ablation trials were conducted on MDA-MB-231 cell cultures seeded in 48 well plates (BD Biosciences). Wells were initially seeded with 150 µl of approximately 6750 cells/well and incubated at 37 °C

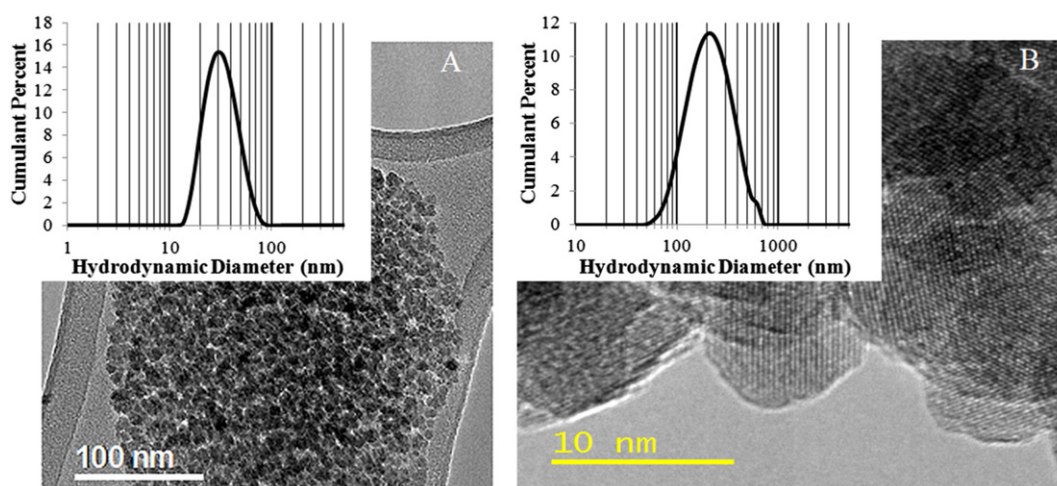


Fig. 1. A) TEM image of PAA-Fe₃O₄. B) TEM image of UC-Fe₃O₄.

in a 5% CO₂ to allow for cellular adhesion. HBSS was used as the dispersant for the PAA-Fe₃O₄ during irradiation after the adhesion period. Upon addition of the PAA-Fe₃O₄, the specific well was subjected to a 38.5 kW/m², 785 nm NIR laser for 15 min in a 37 °C controlled environment. A positive control was established by subjecting seeded wells to only HBSS for 15 min, and the impact of the 785 nm NIR laser was quantified by applying the 38.5 kW/m², 785 nm NIR laser for 15 min to a well with pure HBSS. Upon completion of hyperthermic trials, HBSS dispersed PAA-Fe₃O₄ was replaced with 150 μl of complete-DMEM. Cellular viability was quantified 48 h post-ablation to allow for the completion of necrotic and apoptotic events.

2.9. Viability quantification

The Promega® CellTiter-Glo® Luminescent Cell Viability Assay was used to quantify cellular viability. 150 μl of cell lysis buffer was added to test well following the 48 hour period. After addition of the lysis buffer, the plate was subjected to orbital shaking for 10 min and then allowed to rest for an additional 10 min. After this time period, 200 μl aliquots were removed from the 300 μl total volume of each well and pipetted into a 96 white well plate. One well in the 96 white well plates was exclusive to one well in the 48 well plates. Relative luminescence was quantified by a luminometer.

3. Results

Transmission electron microscopy (TEM) images of PAA-Fe₃O₄ and UC-Fe₃O₄ with respective hydrodynamic diameter distributions quantified through dynamic light scattering are shown in Fig. 1. Size distributions indicate fairly monodisperse samples. The high-resolution TEM image of UC-Fe₃O₄, with lattice fringe spacing characteristic of the structure of Fe₃O₄, has a morphology similar to that of PAA-Fe₃O₄. Insets depict hydrodynamic diameter distributions for the respective nanoparticle systems dispersed in phosphate buffered to a pH of 7.2.

Size distributions of PAA-Fe₃O₄ are shown in Table 1 post-48 h of incubation in HBSS and complete-DMEM. Due to the high electrical conductivity of the buffered solutions, zeta potentials were quantified using de-ionized water. PAA-Fe₃O₄ displayed two peaks in the zeta potential measurements. While not normally observed, the dual peaks may be caused by the variation in association of surface ions with the carboxylic acid functional side chain and its respective conjugate base as the pKa of PAA is reported at 6.8 [23]. One prominent peak is observed at -40 mV while the second prominent peak is observed at -2 mV. Average zeta potentials for PAA-Fe₃O₄ and UC-Fe₃O₄ appeared to be within or close to the region of moderate stability [24].

The stability of PAA-Fe₃O₄ and UC-Fe₃O₄ in HBSS and complete-DMEM was quantified using a Malvern Zetasizer Nano ZS with DLS capabilities. Solutions of PAA-Fe₃O₄ and UC-Fe₃O₄ were created using serial dilutions. After creation of the appropriate concentrations, solutions were sonicated for 40 min directly prior to measurements. In order to characterize the aggregation behaviors in a biologically similar environment, PAA-Fe₃O₄ and UC-Fe₃O₄ dispersions were incubated for 48 h at 37 °C following initial measurements. Hydrodynamic diameters quantified through dynamic light scattering post-48 h of incubation in complete-DMEM revealed a size of 46 ± 21 nm and 360 ± 170 nm for PAA-Fe₃O₄ and UC-Fe₃O₄ respectively showing non-significant aggregation.

It is important to note that the aggregation of UC-Fe₃O₄ present when HBSS is used as a dispersant. Initially, UC-Fe₃O₄ was observed to possess a hydrodynamic diameter of 190 ± 80 nm when dispersed in phosphate buffer. Following the 48 h/37 °C incubation period in HBSS, the observed hydrodynamic diameter for UC-Fe₃O₄ was within the micrometer regime at 4300 ± 1900 nm. While a difference in salt species and concentrations exists between HBSS and phosphate buffer, the effects on particle size are decoupled by establishing a relative percent increase in size relative to PAA-Fe₃O₄. PAA-Fe₃O₄ samples under similar conditions possessed hydrodynamic diameters of 40 ± 18 nm and 34 ± 11 nm respectively. This comparison revealed significant aggregation of UC-Fe₃O₄ relative to PAA-Fe₃O₄

Table 1

Hydrodynamic diameters of PAA-Fe₃O₄ and UC-Fe₃O₄ in HBSS, complete-DMEM, and phosphate buffer, and zeta potential post-sonication in de-ionized water.

| | Post-sonication | | Post-48 h of incubation | | Post-sonication | | |
|-----|------------------|------------------|-------------------------|------------------|-----------------------------|-------|---------------------|
| | Media | | Media | | Phosphate buffer (pH = 7.2) | | DI-water |
| | Z-average (d·nm) | Z-average (d·nm) | Z-average (d·nm) | Z-average (d·nm) | Z-average (d·nm) | PDI | Zeta potential (mV) |
| PAA | 40 ± 18 | 34 ± 11 | 46 ± 21 | | 30 ± 10 | 0.115 | -32 ± 19 |
| UC | 310 ± 150 | 4300 ± 1900 | 360 ± 170 | | 190 ± 80 | 0.188 | 37 ± 7 |

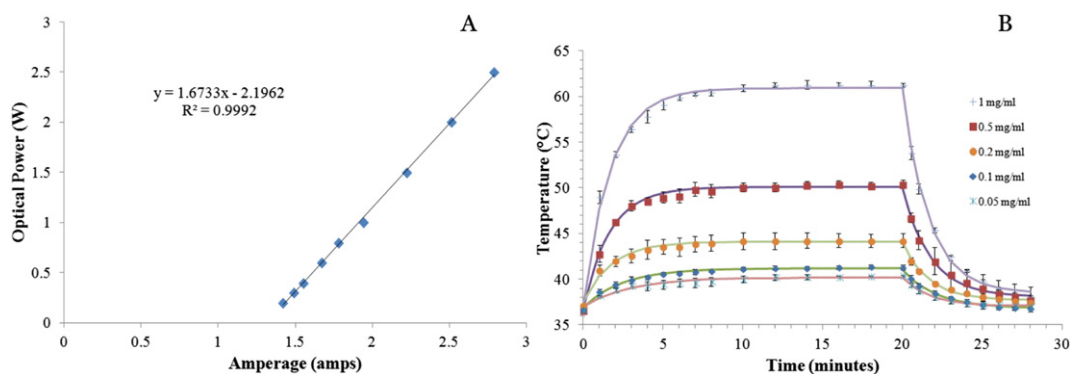


Fig. 2. A) Linear relationship between supplied current and optical power output. B) Heating curves for 150 µl of PAA-Fe₃O₄. Photothermal effect generated through application of 38.5 kW/m², 785 nm NIR laser for 15 min. Temperature measured through IR thermal imaging by a FLIR-T640.

with a p -value < 0.0001 , indicating that the PAA coating had effectively stabilized the uncoated nanoparticles when considering HBSS as a dispersant and allowed for the utilization of HBSS during *in-vitro* hyperthermic trials.

A system with the 785 nm lasers was constructed with diodes in parallel and powered by a Hewlett Packard 10 A/60 volt power supply. Power output was quantified and plotted against supplied amperage to establish a relation between supplied amperage and optical power.

Heating and cooling curves for the PAA-Fe₃O₄ samples were developed for a 38.5 kW/m², 785 nm laser for 20 min (Fig. 2B) to investigate an appropriate optical intensity that may be used in combination with PAA-Fe₃O₄ solutions in order to effectively thermally ablate cancer cells *in-vitro* through the induction of the photothermal effect. Cooling curves were assessed for 8 min following the 20 minute subjection period. An appropriate optical intensity for initial investigations was

chosen with respect to the PAA-Fe₃O₄ innate toxicity measurements detailed in Fig. 3.

Solutions of PAA-Fe₃O₄ and UC-Fe₃O₄ nanoparticles dispersed in complete-DMEM were created to encompass a near 10,000 fold concentration range. Fig. 3A shows the concentration dependent cellular viability curve for PAA-Fe₃O₄. Significant differences from the positive control wells are observed beginning at 1 mg/ml. Fig. 3B shows the concentration dependent cellular viability curve for UC-Fe₃O₄. Significant differences from the positive control well are observed beginning at 0.05 mg/ml. This is in good agreement with previous literature [9,10, 25]. This is a stark decrease in innate toxicity between the PAA-Fe₃O₄ and UC-Fe₃O₄ nanoparticles, and is outlined through the juxtaposition of the viability curves in Fig. 3C. An F-test was conducted through Graph Pad to compare the significance of the innate toxicity curve shift between the two nanoparticle constructs. A significant curve shift exists with a p -value < 0.0001 . Significant differences between the two

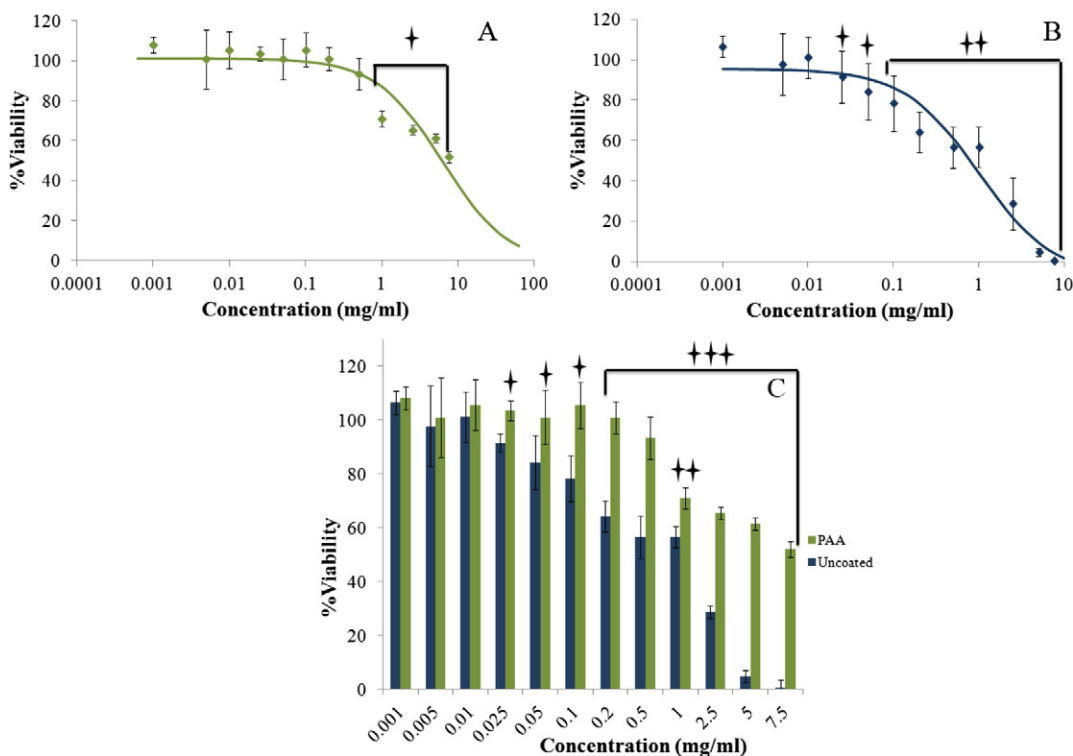


Fig. 3. A) Innate toxicity of poly(acrylic acid) coated magnetite nanoparticles suspended in complete-DMEM. Innate toxicity was conducted over a 48 hour time period. Significant differences from unpaired t-test: one star— $p < 0.0001$. B) Innate toxicity of uncoated magnetite nanoparticles suspended in complete-DMEM. Innate toxicity was conducted over a 48 hour time period. Significant differences from unpaired t-test: one star— $p < 0.05$ and two stars— $p < 0.001$. C) Comparison of PAA-Fe₃O₄ and UC-Fe₃O₄ innate toxicity curves. Curve comparison completed using F-test, p -value < 0.0001 , significant differences between UC-Fe₃O₄ and UC-Fe₃O₄: one star— $p < 0.05$, two stars— $p < 0.01$, and three stars— $p < 0.0001$.

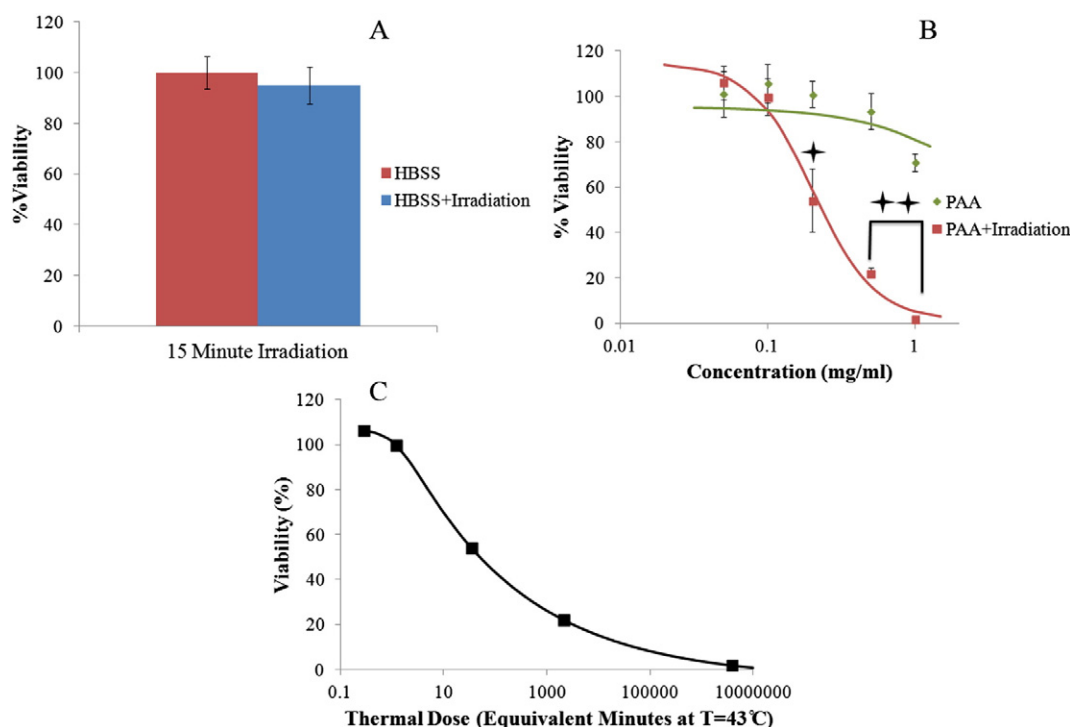


Fig. 4. A) Impact of 38.5 kW/m^2 , 785 nm NIR laser on MDA-MB-231 well cultures. Cell cultures were irradiated for 15 min under $150 \mu\text{l}$ of HBSS (blue bar) and compared against the positive control of cells subjected to only $150 \mu\text{l}$ of HBSS (red bar). B) Viability curve of MDA-MB-231 cell cultures 48 h after hyperthermic ablation compared against innate toxicity. Photothermal effect generated using poly(acrylic acid) coated magnetite nanoparticles subjected to a 38.5 kW/m^2 , 785 nm NIR laser for 15 min. Significant differences from unpaired t-test: one star— $p = 0.006$ and two star— $p < 0.0001$. C) Hyperthermic viability curve for PAA- Fe_3O_4 plotted against logarithm of calculated thermal dose from heating curves. Fit completed through a 5-parameter fit for asymmetric sigmoidal functions.

nanoparticle constructs were observed to begin at 0.025 mg/ml . As concentrations less than 1 mg/ml for the PAA- Fe_3O_4 had an insignificant impact on cell viability, a corresponding optical intensity was selected for 0.5 mg/ml which imparts an appropriate thermal dose over the heating period, 20 min, for a significant reduction in cell viability [26].

An enclosed, temperature-controlled environment was used during hyperthermic ablation trials. With an optical intensity of 38.5 kW/m^2 , it was important to assess the impact of the optical intensity on *in vitro* cultures. Fig. 4A shows the impact of the 38.5 kW/m^2 , 785 nm laser on MDA-MB-231 *in-vitro* cultures. No significant impact from the optical intensity was observed over the 20 minute irradiation periods.

Results of the hyperthermic ablation trials of MDA-MB-231 *in-vitro* cultures are detailed in Fig. 4B. From Fig. 4B, significant viability loss of *in-vitro* cultures was observed at concentrations above 0.1 mg/ml . *In-vitro* wells solely subjected to the 38.5 kW/m^2 , 785 nm laser were used as the positive control wells. The significance in the curve shift between the innate toxicity and the hyperthermic ablation curves compared in Fig. 4B was quantified through an F-test. It was found that the two curves in the region of PAA- Fe_3O_4 concentrations used were significantly shifted with a p -value < 0.0001 .

UC- Fe_3O_4 hyperthermic ablation trials were not completed as innate toxicity issues and aggregation limitations of UC- Fe_3O_4 in HBSS disallowed conduction of hyperthermic ablation trials. Therefore, thermal doses for UC- Fe_3O_4 in equivalent minutes at 43°C were quantified from the measured heating curves using de-ionized water. Fig. 4C models the 5-parameter asymmetric sigmoidal dose response curve generated for the observed viability post-hyperthermic ablation against equivalent minutes at 43°C [26]. Significant differences in the hyperthermic ablative efficacy were then examined between the PAA- Fe_3O_4 and UC- Fe_3O_4 nanoparticles using this equivalent minute relationship.

Fig. 5 quantifies hyperthermic efficacy through the expected viability of *in-vitro* culture purely from thermal dose from 0.5 mg/ml PAA- Fe_3O_4 and UC- Fe_3O_4 nanoparticle solutions. Thermal dose was

calculated using the method described by Sapareto and Dewey [26]. Calculated thermal doses for PAA- Fe_3O_4 and UC- Fe_3O_4 were used in conjunction with the 5-parameter asymmetric sigmoidal fit modeled in Fig. 4C to calculate the expected viability. It was determined that no significant difference existed between the PAA- Fe_3O_4 and UC- Fe_3O_4 nanoparticles in hyperthermic efficacy. Furthermore, with consideration of the innate toxicities of the PAA- Fe_3O_4 and UC- Fe_3O_4 nanoparticles, it is concluded that the PAA- Fe_3O_4 particles are far superior to UC- Fe_3O_4 for use in hyperthermic ablation treatments.

4. Discussion

Particle diameter plays an important role in renal and mononuclear phagocyte system clearance avoidance [27]. Tabulated hydrodynamic diameters for PAA- Fe_3O_4 dispersed in complete-DMEM indicate that the particular synthesis method used to coat the magnetite nanoparticles with PAA generates a core-shell system which may be applicable for EPR utilization *in-vivo*. Z-average sizes were determined in complete-DMEM using 0.5 mg/ml of PAA coated and uncoated magnetite nanoparticles at 0 and 48 h. Sonication of the particle systems was completed prior to the initial measurement. The Z-average hydrodynamic diameters for UC- Fe_3O_4 and PAA- Fe_3O_4 did not show significant changes over the 48 hour period when dispersed in complete-DMEM. Conversely, a significant difference in the percent change of the hydrodynamic diameter was observed for UC- Fe_3O_4 dispersed in HBSS relative to PAA- Fe_3O_4 in HBSS for 48 h at 37°C , with a p -value < 0.0001 .

Furthermore, the innate toxicity of PAA- Fe_3O_4 reveals a modification by the PAA coating to the biological behaviors of the iron oxide core. MDA-MB-231 cell cultures subjected to UC- Fe_3O_4 at a concentration range from $1 \mu\text{g/ml}$ – 7.5 mg/ml revealed significant toxicity beginning at $50 \mu\text{g/ml}$ with a p -value = 0.03, while PAA- Fe_3O_4 elicited significant toxicity beginning at 1.0 mg/ml for the MDA-MB-231 cell cultures with a p -value < 0.0001 . A curve comparison was completed through Graph Pad using an F-test to examine the curve shift in the PAA- Fe_3O_4 innate

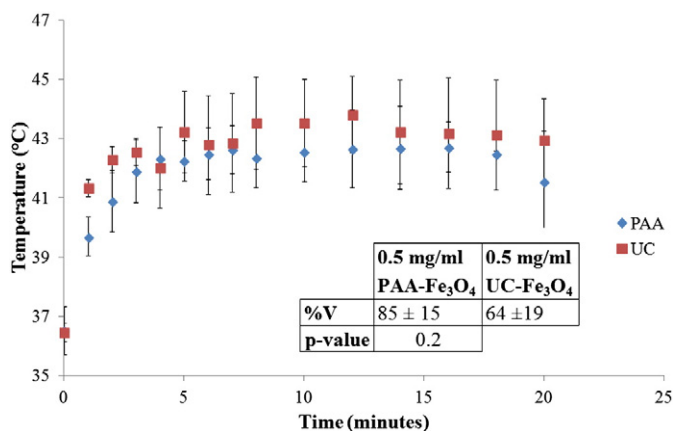


Fig. 5. Heating curves for 0.5 mg/ml PAA-Fe₃O₄ and UC-Fe₃O₄ solutions dispersed in pure de-ionized water subjected to a 3.5 kW/m², 785 nm laser. Inset: Expected viability and standard deviations calculated from thermal dose using the 5-parameter sigmoidal fit modeled in Fig. 4C.

toxicity juxtaposed with the UC-Fe₃O₄ innate toxicity. The F-test showed a significant shift in the PAA-Fe₃O₄ innate toxicity curve relative to that of the UC-Fe₃O₄ with a p-value < 0.0001. Thus, the PAA coating has effectively increased the therapeutic window for the Fe₃O₄ nanoparticles. Investigation of photothermal effect on MDA-MB-231 cell cultures revealed a significant reduction in *in-vitro* cellular viability beginning at 0.2 mg/ml relative to the positive control. At this concentration, utilizing an irradiance of 38.5 kW/m² at 785 nm, a steady state temperature near 43 °C is reached and is expected to induce irreversible thermal damage [26]. Furthermore, a significant reduction in *in-vitro* cellular viability induced by the photothermal effect relative to the quantified innate toxicity is observed to begin at 0.2 mg/ml.

5. Conclusion

Quantification of uncoated magnetite nanoparticle innate toxicity using MDA-MB-231 human mammary gland adenocarcinoma revealed similar trends reported in previous literature with a significant impact beginning at 50 µg/ml [9,10]. As future implications for nanomedicine lie heavily in the clinical regime, it is imperative that efficacy is maximized at the *in-vitro* stage for clinical relevance. An effective nanoparticle construct must not elicit significant toxicity until application of mediating factors. Uncoated magnetite therefore provides a poor vector for photothermal therapy due to the relatively high toxicity observed *in-vitro*.

Successful modification of uncoated magnetite nanoparticle by poly(acrylic acid) encapsulation is observed through the shift in zeta potential tabulated in Table 1. As a direct result of this polymeric encapsulation a prominent modification to the toxicity profile is observed, leading to a near 10 fold increase in the median lethal dose and demonstrates the high applicability for PAA to be utilized as a coating agent. Furthermore, the PAA coating may provide highly convenient reactive groups for moiety conjugation as capping surface is primarily populated with carboxylate functional groups at physiological pH [23]. From the heating profile shown in Fig. 2 the minimum concentration of PAA-Fe₃O₄ required to significantly affect cellular viability is 0.2 mg/ml upon application of a 38.5 kW/m², 785 nm laser; moreover this concentration does not significantly innately impact MDA-MB-231 viability *in-vitro*. This functionalized nano-vector synthesized through the aforementioned procedure provides a highly applicable and effective nanoparticle system for optical hyperthermia due to the coating of the magnetite nanoparticles with poly(acrylic acid) and may be applicable for utilization of the *in-vivo* specific EPR effect. Without this coating, the uncoated magnetite would be largely ineffective due to the high toxicity relative to the concentration required for inducing significant viability loss by optical hyperthermia.

Financial disclosure

This research is supported by a grant from National Science Foundation with the award number EEC-1343568. The work at Tongji University was supported by grants from Shanghai Nanotechnology Promotion Center (Grant Nos.11 nm0506100 and 12 nm0501201) and the National Natural Science Foundation of China (No. 51173135).

All work is original and no portion has been previously published. All parties involved possessed no conflict of interest and participated in the enclosed research purely out of interest for the advancement of scientific knowledge.

References

- [1] C. Wang, J. Chen, T. Talavage, J. Irudayaraj, Gold nanorod/Fe₃O₄ nanoparticle "nano-pearl-necklaces" for simultaneous targeting, dual-mode imaging, and photothermal ablation of cancer cells, *Angew. Chem.* 121 (2009) 2797–2801.
- [2] A.M. Gobin, et al., Near-infrared resonant nanoshells for combined optical imaging and photothermal cancer therapy, *Nano Lett.* 7 (2007) 1929–1934.
- [3] A.R. Lowery, A.M. Gobin, E.S. Day, N.J. Halas, J.L. West, Immunonanoshells for targeted photothermal ablation of tumor cells, *Int. J. Nanomedicine* 1 (2006) 149.
- [4] J.T. Robinson, et al., Ultrasmall reduced graphene oxide with high near-infrared absorbance for photothermal therapy, *J. Am. Chem. Soc.* 133 (2011) 6825–6831.
- [5] M. Chu, et al., Near-infrared laser light mediated cancer therapy by photothermal effect of Fe₃O₄ magnetic nanoparticles, *Biomaterials* 34 (2013) 4078–4088.
- [6] V.P. Pattani, J.W. Tunnell, Nanoparticle-mediated photothermal therapy: a comparative study of heating for different particle types, *Lasers Surg. Med.* 44 (2012) 675–684.
- [7] G. Liu, J. Ma, J. Liu, Photothermal effect for Fe₃O₄ nanoparticles contained in micelles induced by near-infrared light, *J. Shanghai Jiaotong Univ. (Sci.)* 17 (2012) 730.
- [8] Q. Tian, et al., Sub-10 nm Fe₃O₄@Cu₂-xS core-shell nanoparticles for dual-modal imaging and photothermal therapy, *J. Am. Chem. Soc.* 135 (23) (2013) 8571–8577.
- [9] B. Ankamwar, et al., Biocompatibility of Fe₃O₄ nanoparticles evaluated by *in vitro* cytotoxicity assays using normal, glia and breast cancer cells, *Nanotechnology* 21 (2010) 075102.
- [10] S. Naqvi, et al., Concentration-dependent toxicity of iron oxide nanoparticles mediated by increased oxidative stress, *Int. J. Nanomedicine* 5 (2010) 983.
- [11] M. Mahmoudi, A. Simchi, M. Imani, A.S. Milani, P. Stroeve, An *in vitro* study of bare and poly(ethylene glycol)-co-fumarate-coated superparamagnetic iron oxide nanoparticles: a new toxicity identification procedure, *Nanotechnology* 20 (2009) 225104.
- [12] O. Akhavan, E. Ghaderi, H. Emamy, Nontoxic concentrations of PEGylated graphene nanoribbons for selective cancer cell imaging and photothermal therapy, *J. Mater. Chem.* 22 (2012) 20626–20633.
- [13] G. Huang, et al., Superparamagnetic iron oxide nanoparticles: amplifying ROS stress to improve anticancer drug efficacy, *Theranostics* 3 (2013) 116.
- [14] N. Kamal, et al., Light-activated cytotoxic compounds from Malaysian microorganisms for photodynamic therapy of cancer, *Antonie Van Leeuwenhoek* 95 (2009) 179–188.
- [15] P.J. Bednarski, et al., Light-activated destruction of cancer cell nuclei by platinum diazide complexes, *Chem. Biol.* 13 (2006) 61–67.
- [16] A.K. Iyer, G. Khaled, J. Fang, H. Maeda, Exploiting the enhanced permeability and retention effect for tumor targeting, *Drug Discov. Today* 11 (2006) 812–818.
- [17] H. Maeda, J. Wu, T. Sawa, Y. Matsumura, K. Hori, Tumor vascular permeability and the EPR effect in macromolecular therapeutics: a review, *J. Control. Release* 65 (2000) 271–284.
- [18] H. Maeda, The enhanced permeability and retention (EPR) effect in tumor vasculature: the key role of tumor-selective macromolecular drug targeting, *Adv. Enzym. Regul.* 41 (2001) 189–207.
- [19] S. Acharya, S.K. Sahoo, PLGA nanoparticles containing various anticancer agents and tumour delivery by EPR effect, *Adv. Drug Deliv. Rev.* 63 (2011) 170–183.
- [20] F. Alexis, E. Pridgen, L.K. Molnar, O.C. Farokhzad, Factors affecting the clearance and biodistribution of polymeric nanoparticles, *Mol. Pharm.* 5 (2008) 505–515.
- [21] T.J. Dougherty, et al., Photodynamic therapy, *J. Natl. Cancer Inst.* 90 (1998) 889–905.
- [22] H. Xu, C. Cheng, D. Chen, H. Gu, Magnetite nanocrystal clusters with ultra-high sensitivity in magnetic resonance imaging, *ChemPhysChem* 13 (2012) 336–341.
- [23] K. Lienkamp, C.F. Kins, S.F. Alfred, A.E. Madkour, G.N. Tew, Water-soluble polymers from acid-functionalized norbornenes, *J. Polym. Sci. A Polym. Chem.* 47 (2009) 1266–1273.
- [24] C. Freitas, R.H. Müller, Effect of light and temperature on zeta potential and physical stability in solid lipid nanoparticle (SLN™) dispersions, *Int. J. Pharm.* 168 (1998) 221–229.
- [25] T.R. Pisanic II, J.D. Blackwell, V.I. Shubayev, R.R. Fiñones, S. Jin, Nanotoxicity of iron oxide nanoparticle internalization in growing neurons, *Biomaterials* 28 (2007) 2572–2581.
- [26] S.A. Sapareto, W.C. Dewey, Thermal dose determination in cancer therapy, *Int. J. Radiat. Oncol. Biol. Phys.* 10 (1984) 787–800.
- [27] G. Storm, S.O. Belliot, T. Daemen, D.D. Lasic, Surface modification of nanoparticles to oppose uptake by the mononuclear phagocyte system, *Adv. Drug Deliv. Rev.* 17 (1995) 31–48.